AN EIGHT-NODE HEXAHEDRON ELEMENT WITH REDUCTION OF SHAPE SENSITIVITY AND HIGH PERFORMANCES IN SHELL APPLICATIONS

A. Dósa
University TRANSILVANIA Braşov, Faculty of Civil Engineering, 5 Turnului Street, 500152 Braşov, Romania
adamd@rdslink.ro

ABSTRACT
In this paper an eight-node hexahedron finite element is presented. This type of elements are useful for modeling structures with shell and 3D configuration without the need to connect solid elements to shell nodes. The element is based on the displacement mode separation method, which is an unsymmetrical stress-hybrid formulation, with assumed boundary displacements and displacement derived internal stresses. The stress field parameters are grouped on constant stress modes, bending modes and higher order stress modes and are linked to the nodal displacements of the element. The element can reproduce exactly all the six constant strain modes, has correct rank and is of high accuracy in complex applications. The numerical results for known beam, plate and curved shell test problems show an excellent behavior of the proposed element, with a very low shape sensitivity. In some cases, for example beams and plates in constant bending, the elements are even insensitive to distortion.

Keywords: Eight-node solid element, unsymmetrical finite element formulations, shape sensitivity.

1. INTRODUCTION
The eight-node solid elements with translational degrees of freedom, like the corresponding four-node quadrilateral elements exhibit a high shape sensitivity in special in bending. This drawback limits the use of these elements in curved shell and curved beam applications, where trapezoidal shaped elements are necessary. According to MacNeal's theorem [3], a four-node trapezoidal element cannot have locking-free in-plane bending and constant deformation capability, while simultaneously satisfying reciprocity and the compatibility of the nodal displacements. In the literature several efforts were made to improve the performances of quadrilaterals and to extend the results to hexahedron elements. Many of the approaches are based on relaxing some of the terms of MacNeal's theorem.
For example K.Y.Sze [10] introduces a selective scaling procedure that judiciously reduces the stiffness arising from the two bending stress/strain modes in the four-node element. Another way to improve the bending capability of distorted quadrilateral elements is given by X.M.Chen et al. [1] by using the quadrilateral area coordinate method. The resulting elements fail to pass the strict patch test, but pass patch tests in a weak sense.
The H8MS solid element presented in this paper is based on the method of separation of displacement modes, which is an unsymmetrical formulation. An unsymmetrical formulation given by S.Rajendran and K.M.Liew [9], E.T.Ooi, S.Rajendran and J.H.Yeo [6] led to the development of successful 8-node plane elements and 20-node hexahedron elements with high distortion tolerance and very good performances. In their formulation, the authors are using two different sets of functions, one set as weighting functions to enforce compatibility and one as shape functions for the completeness of the displacement field.
The formulation presented in this paper, instead of the second set of shape functions, uses displacement modes. The elements based on this approach are capable to reproduce exactly the nodal forces corresponding to any of the displacement modes used in the formulation of the element. As a result, the patch test is passed without any other special measures. Also the elements give exact answers for constant bending and torsion corresponding to the axes of the elements. Because there is no contamination between modes, no parasitic energy arises in the elements and hence high coarse mesh accuracy resulted for all the numerical test problems.

2. SOME REMARKS ON THE ISSUE OF INTER-ELEMENT CONTINUITY
An introduction of the herein formulation can be done with the help of the stress-hybrid principle (T.H.H.Pian [7], [8], C.Felippa [2]).

$$\Pi(\boldsymbol{\sigma},\mathbf{d}) = -\frac{1}{2}\int_{\Omega}\boldsymbol{\sigma}^T\mathbf{C}\boldsymbol{\sigma}\,d\Omega + \int_{\Gamma}\mathbf{d}^T\boldsymbol{\sigma}_{\mathbf{n}}\,d\Gamma - \int_{\Gamma^t}\mathbf{d}^T\hat{\mathbf{t}}\,d\Gamma \rightarrow stat. \qquad (1)$$

Here $\boldsymbol{\sigma}$ is an assumed stress field in internal equilibrium in the domain Ω in the absence of body forces, $\boldsymbol{\sigma}_{\mathbf{n}} = \boldsymbol{\sigma}^T\mathbf{n}$ is the surface traction on the boundary Γ, $\mathbf{C}$ is the elastic compliance, $\mathbf{d}$ is the boundary displacement field, and $\hat{\mathbf{t}}$ stands for the prescribed boundary tractions on Γ^t. If $\boldsymbol{\sigma}$ is a displacement derived stress field

$\boldsymbol{\sigma} = \boldsymbol{\sigma}^{\mathbf{u}} = \mathbf{C}^{-1}\mathbf{D}\,\mathbf{u}$, where **D** is the symmetric gradient operator, and **u** is the assumed internal displacement field, equation (1) can be rewritten as:

$$\Pi(\mathbf{u},\mathbf{d}) = -\frac{1}{2}\int_{\Gamma} \boldsymbol{\sigma}_{\mathbf{n}}^{\mathbf{u}T}\mathbf{u}\,d\Gamma + \int_{\Gamma} \mathbf{d}^{T}\boldsymbol{\sigma}_{\mathbf{n}}^{\mathbf{u}}\,d\Gamma - \int_{\Gamma^{t}} \mathbf{d}^{T}\hat{\mathbf{t}}\,d\Gamma \rightarrow stat. \tag{2}$$

Rendering functional (2) stationary gives:

$$\int_{\Gamma} \delta\boldsymbol{\sigma}_{\mathbf{n}}^{\mathbf{u}T}(\mathbf{d}-\mathbf{u})\,d\Gamma = 0, \tag{3}$$

$$\int_{\Gamma} \delta\mathbf{d}^{T}\boldsymbol{\sigma}_{\mathbf{n}}^{\mathbf{u}}\,d\Gamma - \int_{\Gamma^{t}} \delta\mathbf{d}^{T}\hat{\mathbf{t}}\,d\Gamma = 0. \tag{4}$$

Relation (3) enforces continuity on the Γ boundary in a weak sense and must hold for any admissible $\delta\boldsymbol{\sigma}^{\mathbf{u}}$ virtual stress field. Relation (3) is a weak conformity condition. Relation (4) introduces the static equilibrium conditions and must hold for any $\delta\mathbf{d}$ virtual boundary displacement field.

Using relations (3) and (4) at finite element level leads to symmetric stress-hybrid elements. In this case displacements **d** are linked to the nodal displacements and are conforming, while displacements **u** have free parameters and are nonconforming. More precisely, the displacements **u** corresponding to some high order modes of the element are nonconforming. The displacements **u** in the lower order modes are conforming and on the boundary coincide with the corresponding **d** displacements. (Here conformity stands for the capability of the element to provide continuity for any displacements of the nodes.) Enforced at finite element level, relation (3) becomes a weak conformity condition. For some regular shaped elements relation (3) has no effect, since the boundary integral is zero for $\delta\boldsymbol{\sigma}_{\mathbf{n}}^{\mathbf{u}}$ in any mode and (**d**-**u**) in any mode. In these cases free incompatible displacements can develop. Unfortunately in the case of distorted shapes this relation is too restrictive and introduces excessive energy. The finite elements based on relations (3) and (4) are weak conforming and suffer of a class of locking, that can be named weak conformity locking. This kind of locking is produced by the incorrect cinematic link between nodal and modal displacements.

3. THE DISPLACEMENT MODE SEPARATION METHOD

If the nonconforming displacements **u** are linked to the nodal displacements, neglecting condition (3) leads to an unsymmetrical formulation. In the remaining relation (4) functions $\delta\mathbf{d}$ are weighting functions and are not effectively used to build the solution. In this case the weak conformity condition is replaced by a built-in nodal continuity condition and the inter-element continuity is no more strictly controlled. However due to the less restrictive conditions, even pointwise inter-element continuity is possible, like in the case of the quadrilateral elements of figure 1. a), while the corresponding symmetric formulation leads to poor results. In the case of symmetric formulation elements of distorted shape, inter-element continuity can be achieved only for displacements corresponding to the conforming subspace of **u.** In other words a part of the approximation capability of the symmetric elements cannot be fully exploited because of the weak conformity condition. Unsymmetrical elements can do more. The degree of inter-element continuity guaranteed by unsymmetrical elements depends on the degree of approximation of the variation of displacement states between neighboring elements, by the whole assumed internal displacement space of the elements. If the variation of the displacement field is smooth, the performances of the unsymmetrical elements are very high.

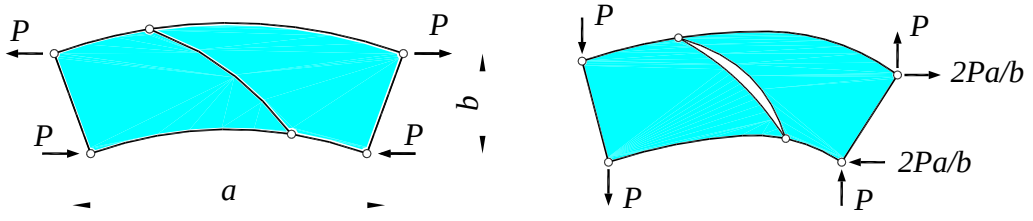

a) constant bending b) linear bending

Figure 1. Deformed adjacent elements

On the other hand, it can be shown that dropping the weak conformity conditions, while using nodal displacement linked nonconforming shape functions, introduces small errors.

Choosing the nonconforming displacements in a way to have the displacement derived stresses in homogenous equilibrium, leads to the use of deformation modes. These deformation modes must be completed with the rigid body movement modes. Deformation modes and rigid body modes together are the displacement modes.

Relation (4) applied to the conforming boundary displacements and the (nonconforming) deformation modes leads to a nodal force – nodal displacement relation, which separates the deformation modes, such that all the modes are correctly reproduced by the element from the corresponding nodal displacements.
The assumed boundary displacements are:

$$\delta\mathbf{d} = \mathbf{P}\,\delta\mathbf{a}\,, \tag{5}$$

where **P** is the matrix of the appropriate conforming shape functions and $\delta\mathbf{a}$ is the nodal virtual displacement vector. The nonconforming displacements are:

$$\mathbf{u} = \mathbf{N}\,\mathbf{q}\,, \tag{6}$$

where **N** is the corresponding matrix of interpolation and **q** is the vector of modal displacements.
The internal stress field is:

$$\boldsymbol{\sigma}^{\mathbf{u}} = \mathbf{C}^{-1}\mathbf{D}\mathbf{u} = \mathbf{C}^{-1}\mathbf{D}\,\mathbf{N}_d\,\mathbf{q}_d = \mathbf{S}\,\mathbf{q}_d\,, \tag{7}$$

where $\mathbf{N}_d$ and $\mathbf{q}_d$ are the partitions of **N** and **q** respectively corresponding to the deformation modes.
The boundary tractions $\boldsymbol{\sigma}_{\mathbf{n}}$ are computed from the interior stress field, using the traction-stress matrix **T** built from the components of the normal to the boundary of the element.

$$\boldsymbol{\sigma}_{\mathbf{n}} = \mathbf{T}\boldsymbol{\sigma}\,. \tag{8}$$

The $\mathbf{q}_d$ deformation mode vector can be obtained from the nodal displacement vector **a** of the element.

$$\mathbf{q}_d = \mathbf{H}_d\,\mathbf{a}.\,. \tag{9}$$

The derivation of $\mathbf{H}_d$ matrix involves the construction of the transformation $\mathbf{a} = \mathbf{G}\,\mathbf{q}$, by evaluating the displacement modes at the nodal points. If matrix **G** is nonsingular, inversion gives $\mathbf{H} = \mathbf{G}^{-1}$. $\mathbf{H}_d$ results by extracting from **H** the lines corresponding to the deformation modes.
Inserting (5), (7), (8) and (9) in (4) results:

$$\delta\mathbf{a}^T\mathbf{L}\mathbf{H}_d\mathbf{a} - \delta\mathbf{a}^T\mathbf{f} = 0, \tag{10}$$

In (10) **L** is the leverage matrix, which links the stresses to the nodal forces and **f** is the vector of nodal loadings.

$$\mathbf{L} = \int_{\Gamma^e}\mathbf{P}^T\mathbf{T}\mathbf{S}\,d\Gamma, \tag{11}$$

$$\mathbf{f} = \int_{\Gamma^e}\mathbf{P}^T\hat{\mathbf{t}}\,d\Gamma. \tag{12}$$

Relation (10) must hold for any $\delta\mathbf{a}$. Results the element equilibrium equation

$$\mathbf{k}\mathbf{a} = \mathbf{f} \tag{13}$$

with $\mathbf{k} = \mathbf{L}\mathbf{H}_d$.

4. THE H8MS ELEMENT

The material is assumed homogenous and isotropic with module of elasticity *E* and transversal contraction coefficient μ.

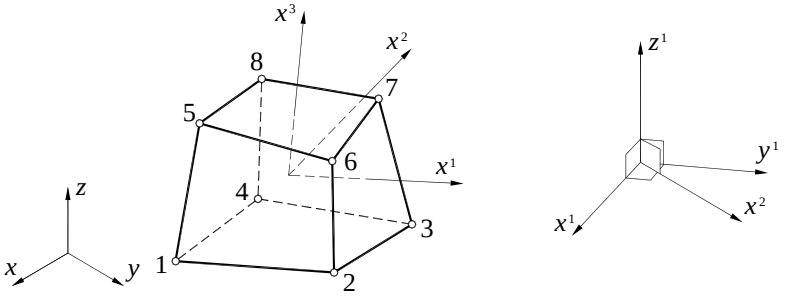

Figure 2. The hexahedron finite element and the reference systems

The geometry of the element is defined with the help of the known triliniar parametric relation:

$$\mathbf{x} = \sum_{i=1}^{8} P_i(\xi,\eta,\zeta)\,\mathbf{x}_i\,, \tag{14}$$

where $\mathbf{x}_i = (x_i,\ y_i,\ z_i)^T$ are the coordinates of the eight nodes of the element. The triliniar shape functions are:

$$P_i(\xi,\eta,\zeta) = \frac{1}{8}(1+\xi\xi_i)(1+\eta\eta_i)(1+\zeta\zeta_i), \tag{15}$$

with the natural coordinates ξ_i, η_i, ζ_i of the nodes:

$$\begin{Bmatrix}\xi\\ \eta\\ \zeta\end{Bmatrix}_{1,2,...8} = \begin{bmatrix}-1 & 1 & 1 & -1 & -1 & 1 & 1 & -1\\ -1 & -1 & 1 & 1 & -1 & -1 & 1 & 1\\ -1 & -1 & -1 & -1 & 1 & 1 & 1 & 1\end{bmatrix}. \tag{16}$$

The three orthogonal right reference systems have their origin in the origin of the natural coordinate system (figure 2). The local x^1, x^2, x^3 axes are tangent to the natural axes in the origin. The local axe y^1 lies in the plane of x^1 x^2 , the local axe z^1 is normal to the x^1 y^1 plane and so on.

The finite element equations follow relations (5),... (13). The boundary displacements are given by equation (5) $\delta\mathbf{d} = \mathbf{P}\ \delta\mathbf{a}$ **,** where **P** is an interpolation matrix built with the shape functions (15). Displacements $\delta\mathbf{d}$ defined with the help of the values of **P** on the boundary of the element are conforming.

The nonconforming internal displacements $\mathbf{u}^i = \mathbf{N}^i\ \mathbf{q}^i$ are defined in the local reference systems i = 1, 2 and 3 with:

$$\mathbf{N}^i = \frac{1}{E}\begin{bmatrix}1 & 0 & x & 0 & x^i y^i & x^i z^i & -(1+\mu)y^i z^i & x^i y^i z^i\\ 0 & -z^i & -\mu y^i & (1+\mu)z^i & -\dfrac{x^{i2}+\mu y^{i2}-\mu z^{i2}}{2} & -\mu y^i z^i & (1+\mu)x^i z^i & 0\\ 0 & y^i & -\mu z^i & (1+\mu)y^i & -\mu y^i z^i & -\dfrac{x^{i2}-\mu y^{i2}+\mu z^{i2}}{2} & (1+\mu)x^i y^i & 0\end{bmatrix} \tag{17}$$

and the corresponding subset of eight modal displacement parameters $\mathbf{q}^i = (q_{8i-7}\ q_{8i-6}\cdots q_{8i})^T$. The modes $q_{8i-7,}\ q_{8i-6}$ are rigid body displacement modes, the modes $q_{8i-5,}\ q_{8i-4}$ are constant stress modes, the modes $q_{8i-3,}\ q_{8i-2}$ are constant bending modes and $q_{8i-1,}\ q_{8i}$ are higher order stress modes.

The stresses derived from the above displacements are:

$$\boldsymbol{\sigma}^{\mathbf{u}i} = \mathbf{S}^i\mathbf{q}_d^i = \begin{Bmatrix}\sigma_{x^i}\\ \tau_{y^i z^i}\end{Bmatrix} = \begin{bmatrix}1 & 0 & y^i & z^i & 0 & \alpha y^i z^i\\ 0 & 1 & 0 & 0 & x^i & 0\end{bmatrix}\begin{Bmatrix}q_{8i-5}\\ q_{8i-4}\\ \vdots\\ q_{8i}\end{Bmatrix}. \tag{18}$$

This stress field fulfills the homogenous equilibrium equations. Except the three q_{8i} high modes, the stresses are simply derived from the displacement modes given by equation (16). Relation $u_{x^i} = \frac{1}{E}x^i y^i z^i$ gives $\sigma_{x^i} = y^i z^i$ and $\tau_{y^i z^i} = -\frac{1}{2(1+\mu)}\left[x^{i2} + \mu(y^{i2} + z^{i2})\right]$. In relation (18) the shear stresses are neglected to not introduce excessive energy. Coefficient α is used for scaling purposes. All the test problems worked well with α=1, except the distortion test in out of plane linear bending. In order to solve this problem, the scaling parameter was set to α=10^{-5}. In other words, in this version, the modes q_{8i} are used only to provide the correct rank of the element stiffness matrix.

Equation (8) is evaluated in the local systems $\boldsymbol{\sigma}_{\mathbf{n}}^{\mathbf{u}i} = \mathbf{T}^i\boldsymbol{\sigma}^{\mathbf{u}i}$.

Matrix **G** results in the following form:

$$\mathbf{G} = \left[\mathbf{R}^1\mathbf{G}^1\ \ \mathbf{R}^2\mathbf{G}^2\ \ \mathbf{R}^3\mathbf{G}^3\right], \tag{19}$$

where matrices $\mathbf{G}^i$ result by evaluating the modal displacements at the nodes of the element and matrices $\mathbf{R}^i$ are the rotation vectors corresponding to the three local reference systems.

The surface integrals from equation (11) are evaluated numerically using four Gauss points on each face of the element. Using nine quadrature points, there were no significant changes in the results.

5. NUMERICAL TESTS

Figure 2 shows a cantilever plate modeled by two elements. The material is characterized by module of elasticity E=1000 and transversal contraction coefficient μ=0.25. The in-plane distortion of the elements is characterized by the eccentricity e. In order to not disturb the stress/strain states in the plate, at the fixed end only the rigid-body movements are eliminated. There are four load cases corresponding to constant in-plane and out-of-plane bending and in-plane and out-of-plane end shear forces (linear bending). The displacements of node "A" normalized by the analytical solutions are given in table 1. It can be observed that there is no distortion sensitivity for constant bending.

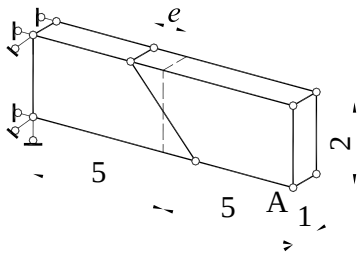

Figure 3. Two-element distortion sensitivity test for in-plane (membrane) and out-of-plane (bending) loading

Table 1. Normalized deflections for the distortion sensitivity test

e	In-plane load cases		Out-of-plane load cases	
	Constant bending	End shear force	Constant bending	End shear force
0	100.00	93.45	100.00	93.67
0.5	100.00	93.63	100.00	94.23
1	100.00	94.18	100.00	96.17
2	100.00	96.36	100.00	103.52
4	100.00	105.10	100.00	124.94

In the figure 4 is presented the model of one eighth of the pinched cylindrical shell problem proposed by MacNeal and Harder [5]. The cylinder is pinched by two diametrically opposite point loads. The deflection under the load is dominated by bidirectional inextensional bending response. Over the rigid diaphragm the boundary conditions are u_x=0, u_z=0. The results reported in table 2 are the vertical displacements under the load normalized with respect to the reference value 1.8248×10^{-5}. The results are compared with that obtained with the isoparametric solid element HEXA8 with reduced integration and six assumed auxiliary strain states [4]. The results are too stiff and the convergence is unsatisfactory because the finite element errors are localized in the vicinity of the load.

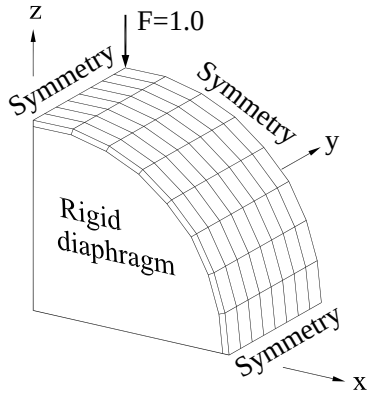

Figure 4. Pinched Cylindrical Shell (E=3000000, μ=0.3, R=300, t=3, L=600)

Table 2. Normalized displacements under the load

Mesh	HEXA8	H8MS
4x4x1	0.1070	0.3222
8x8x1	0.4983	0.7610
16x16x1	0.9133	0.9476
32x32x1	0.9897	0.9956

In the figure 5. the pinched hemisphere test problem is presented. The 18^o hole at the apex is added to allow a regular mesh of hexahedral elements. The shell is loaded by two pairs of orthogonal point loads. For this loading the hole at the apex does not greatly affect the results (it increases the strain energy by less than 2%). A quarter of the whole structure is modeled by a mesh of NxNx1 elements [5]. The convergence is partly affected by inextensional bending overstiffness. The reference solution represents the radial deflection under the point loads and has the value of 0.094.

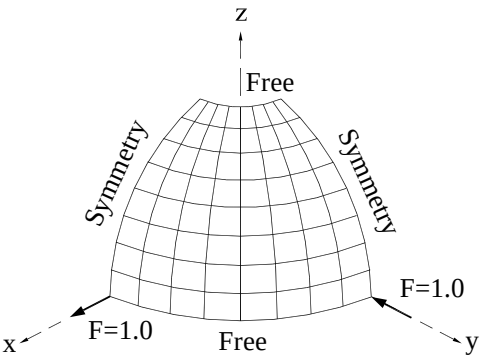

Figure 5. Pinched Hemispherical Shell (E=6.825x10^7, μ=0.3, R=10, t=0.04)

Table 3. Normalized deflections for the Pinched Hemisphere

Mesh	HEXA8	H8MS
8x8x1	0.730	0.8693
12x12x1	0.955	0.9850
16x16x1	-	0.9937

6. CONCLUSIONS

H8MS, an eight-node solid elasticity element has been proposed, which possesses high coarse mesh accuracy. The element is based on the displacement mode separation method. The element passes the constant stress patch tests, shows a low mesh distortion sensitivity and high accuracy in shell applications. However further tests and theoretical investigations are necessary to establish the limits of applicability of the element and to get full confidence in the presented formulation. Also the theoretical basis must be developed to avoid the main shortcoming that limits the applicability of the mode separation method to more complex elements: the need to invert matrix **G,** which has the size of the element stiffness matrix.

REFERENCES

[1] XM.Chen, S.Cen, YQ.Long, ZH.Yao, Membrane elements insensitive to distortion using the quadrilateral area coordinate method, *Computers and Structures* **82**, 35-54, 2004.
[2] C.A.Felippa, *Advanced Finite Element Method*, http://www.devdept.com (2004).
[3] R.H.MacNeal, A theorem regarding the locking of tapered four-noded membrane elements, *Int. J. Numer. Meth. Engng*. **24**, 1793-1799, 1987.
[4] R.H.MacNeal, *Finite Elements: Their Design and Performance*, Marcel Dekker: New York, 1994.
[5] R.H.MacNeal, R.L.Harder, A proposed standard set of problems to test finite element accuracy, *Finite Elem. Anal. Des.*, **1**, 3-22, 1985.
[6] E.T.Ooi, S.Rajendran, J.H.Yeo, A 20-node hexahedral element with enhanced distortion tolerance, *Int. J. Numer. Meth. Engng*., **60**, 2501-2530, 2004.
[7] T.H.H.Pian, Derivation of element stifness matrices by assumed stress distributions. *AIAA Journal*, **2**, 1333-1336, 1964.
[8] T.H.H.Pian, Some notes on the early history of hybrid stress finite element method, *Int. J. Numer. Meth. Engrg*., **47**, 419-425, 2000.
[9] S.Rajendran and K.M.Liew, A novel unsymmetric 8-node plane element immune to mesh distortion under a quadratic displacement field, *Int. J. Numer. Meth. Engng*., **58**, 1713-1748, 2003.
[10] K.Y.Sze, On immunizing five-beta hybrid-stress element models from 'trapezoidal locking' in practical analyses, *Int. J. Numer. Meth. Engng*. **47**, 907-920, 2000.